Perivascular adipose tissue-derived nitric oxide compensates endothelial dysfunction in aged pre-atherosclerotic apolipoprotein E-deficient rats

Nakladal, D; Sijbesma, J W A; Visser, L M; Tietge, U J F; Slart, R H J A; Deelman, L E; Henning, R H; Hillebrands, J L; Buikema, H

Published in:
Vascular pharmacology

DOI:
10.1016/j.vph.2021.106945
10.1016/j.vph.2021.106945

Publication date:
2022

Vascular Pharmacology 142 (2022) 106945

Contents lists available at ScienceDirect

Vascular Pharmacology

journal homepage: www.elsevier.com/locate/vph

Perivascular adipose tissue-derived nitric oxide compensates endothelial dysfunction in aged pre-atherosclerotic apolipoprotein *E*-deficient rats

D. Nakladal [a,*], J.W.A. Sijbesma [b], L.M. Visser [c], U.J.F. Tietge [d,e,f], R.H.J.A. Slart [b,g], L. E. Deelman [a], R.H. Henning [a], J.L. Hillebrands [c], H. Buikema [a]

[a] Department of Clinical Pharmacy and Pharmacology, University of Groningen, University Medical Center Groningen, Hanzeplein 1, 9713GZ Groningen, the Netherlands
[b] Department of Nuclear Medicine and Molecular Imaging, University of Groningen, University Medical Center Groningen, Hanzeplein 1, 9713GZ Groningen, the Netherlands
[c] Department of Pathology & Medical Biology, Pathology division, University of Groningen, University Medical Center Groningen, Hanzeplein 1, 9713GZ Groningen, the Netherlands
[d] Department of Pediatrics, University of Groningen, University Medical Center Groningen, Groningen, the Netherlands
[e] Division of Clinical Chemistry, Department of Laboratory Medicine, Karolinska Institutet, Stockholm, Sweden
[f] Clinical Chemistry, Karolinska University Laboratory, Karolinska University Hospital, SE-141 86 Stockholm, Sweden
[g] Faculty of Science and Technology Biomedical, Photonic Imaging, University of Twente, Enschede, the Netherlands

ARTICLE INFO

Keywords:
Atherosclerosis
Apolipoprotein E
Perivascular adipose tissue
Vascular relaxation
Nitric oxide

ABSTRACT

Background and aims: Atherosclerosis is a major contributor to global mortality and is accompanied by vascular inflammation and endothelial dysfunction. Perivascular adipose tissue (PVAT) is an established regulator of vascular function with emerging implications in atherosclerosis. We investigated the modulation of aortic relaxation by PVAT in aged rats with apolipoprotein E deficiency ($ApoE^{-/-}$) fed a high-fat diet as a model of early atherosclerosis.

Methods and results: $ApoE^{-/-}$ rats (N = 7) and wild-type Sprague-Dawley controls ($ApoE^{+/+}$, N = 8) received high-fat diet for 51 weeks. Hyperlipidemia was confirmed in $ApoE^{-/-}$ rats by elevated plasma cholesterol ($p < 0.001$) and triglyceride ($p = 0.025$) levels. Early atherosclerosis was supported by increased intima/media thickness ratio ($p < 0.01$) and ED1-positive macrophage influx in $ApoE^{-/-}$ aortic intima ($p < 0.001$). Inflammation in $ApoE^{-/-}$ PVAT was characteristic by an increased [18F]FDG uptake ($p < 0.01$), ED1-positive macrophage influx ($p = 0.0003$), mRNA expression levels of CD68 ($p < 0.001$) and IL-1β ($p < 0.01$), and upregulated iNOS protein ($p = 0.011$). The mRNAs of MCP-1, IL-6 and adiponectin remained unchanged in PVAT. Aortic PVAT volume measured with micro-PET/CT was increased in $ApoE^{-/-}$ rats ($p < 0.01$). Maximal endothelium-dependent relaxation (EDR) to acetylcholine in $ApoE^{-/-}$ aortic rings without PVAT was severely impaired ($p = 0.012$) compared with controls, while $ApoE^{-/-}$ aortic rings with PVAT showed higher EDR than controls. All EDR responses were blocked by L-NMMA and the expression of eNOS mRNA was increased in $ApoE^{-/-}$ PVAT ($p = 0.035$).

Conclusion: Using a rat $ApoE^{-/-}$ model of early atherosclerosis, we capture a novel mechanism by which inflammatory PVAT compensates severe endothelial dysfunction by contributing NO upon cholinergic stimulation.

1. Introduction

Cardiovascular diseases remain among the leading causes of death world-wide [1]. The leading factor, coronary heart disease (CHD), was responsible for 8.8 million deaths in 2005 and rose to 9.1 million in 2015 [1]. Moreover, CHD and stroke together constituted 85.1% of

Abbreviations: ApoE, apolipoprotein E; PVAT, perivascular adipose tissue; BAT, brown adipose tissue; WAT, white adipose tissue; EDR, endothelium-dependent relaxation; PE, phenylephrine; L-NMMA, L-N^G-monomethyl arginine; KCl, potassium chloride; E_{max}, efficacy, maximum response at given agonist concentration; CHD, coronary heart disease; LDL, low-density lipoprotein; VLDL, very low-density lipoprotein; [18F]FDG, [18F]2-fluoro-2-deoxy-D-glucose; PET, Positron emission tomography; CT, Computed tomography; FFPE, formalin-fixed, paraffin-embedded; LDLr, low-density lipoprotein receptor; EDHF, endothelium-derived hyperpolarizing factor.

* Corresponding author.
E-mail address: d.nakladal@umcg.nl (D. Nakladal).

https://doi.org/10.1016/j.vph.2021.106945
Received 15 March 2021; Received in revised form 5 November 2021; Accepted 15 November 2021
Available online 18 November 2021

cardiovascular deaths in 2015 globally [1]. The major underlying cause of CHD is atherosclerosis, which is characterized by lipid accumulation in the intima, loss of endothelial function, infiltration of macrophages into the vessel wall, and subsequent formation of foam cells, calcification and vascular inflammation [2]. The formation of a plaque introduces a risk of lumen occlusion and obstruction of blood supply, or rupture and release of a thrombus leading to downstream ischemia or infarction.

Atherosclerosis is often preceded by major risk factors including hyperlipidemia and elevated cholesterol within apolipoprotein B-containing lipoproteins. Moreover, apolipoprotein E (ApoE) is a structural part of all lipoprotein particles and a ligand for cell-surface receptors responsible for the clearance of chylomicrons and very low-density lipoprotein (VLDL) [2]. Mouse and rabbit models of ApoE deficiency are commonly used in atherosclerosis research. They are characterized by elevated plasma concentrations of cholesterol in chylomicron and VLDL fractions and high-fat diet (HFD) can further exacerbate the condition [2]. However due to the small size, mouse models are inherently difficult for accurate imaging of the vasculature and surrounding tissue. Very recently, a rat *ApoE*$^{-/-}$ model combined with a Western-type HFD produced a phenotype that is characterized by hyperlipidemia and mild atherosclerosis which renders this model suitable for molecular imaging of immune infiltrates [3]. In addition, atherogenesis development was previously well described in rat aortas, and the rat aorta has proven a very useful tool for ex vivo assessment of endothelial function [2].

The vascular endothelium plays a central role in atherogenesis, specifically, existing literature describes endothelial damage and dysfunction as a cause of vascular inflammation and plaque formation in mouse models of atherosclerosis and hyperlipidemia [4]. In addition, perivascular adipose tissue (PVAT) has earned recognition as a modulator of vascular functions including constriction, relaxation and remodeling via active secretion of adipocytokines including adiponectin, but also pro-inflammatory mediators such as IL-1β and IL-6 [5–8]. Compared to visceral or white adipose tissue (WAT), thoracic aortic PVAT resembles more closely brown adipose tissue (BAT) with its thermogenic capacity, and an origin lying in progenitor cells that are more closely related to vascular smooth muscle cell progenitors than to adipocyte progenitors [9]. PVAT has been implicated as a factor in atherosclerosis in a dualistic manner: on the one hand it releases mediators that contribute to plaque formation and vascular remodeling, on the other hand it produces adiponectin and prostaglandins with beneficial effects for the endothelium [5,6].

Recently, a closely related study investigated the protective role of PVAT in 4-months old low-density lipoprotein receptor knockout (*LDLr*$^{-/-}$) mice, which was considered a model of early-stage hypercholesterolemia and atherosclerosis [4]. The authors found that *LDLr*$^{-/-}$ thoracic aortic PVAT rescued mild endothelial dysfunction, expressed more eNOS than control PVAT, and produced NO in situ [4]. Moreover, 20-week old *ApoE*$^{-/-}$ rats receiving a Western-type diet exhibited only modest early atherosclerotic characteristics [10]. In light of these findings, we aimed to elucidate the direct contribution of NO derived from PVAT to vasodilatation in organ bath studies by combining apolipoprotein E deficiency and 51-weeks of high-fat diet (HFD) feeding as a model of hyperlipidemia and early atherosclerosis with severe endothelial dysfunction. Ultimately, PVAT-derived NO production which would contribute to preservation of arterial relaxation under pro-atherogenic conditions may be of high clinical relevance, as this novel mechanism may be throttling the progression of atherosclerosis and exacerbation of complications.

Enabled by the commercial availability of a rat model of early atherosclerosis and the accompanying benefits of size and suitability for imaging, we aimed to explore the effects of PVAT on vasomotor function in *ApoE*$^{-/-}$ rats fed HFD for 51 weeks. Progression of dyslipidemia was characterized by plasma levels of cholesterol and triglycerides, and pre-atherosclerosis was assessed by CD68 staining and vessel wall remodeling. In addition, macrophage infiltration and inflammatory markers were detailed in PVAT by means of positron emission tomography (PET), immunohistochemistry and quantification of expression of inflammatory markers [11–14]. Finally, endothelium-dependent relaxation (EDR) studies were performed in thoracic aortic rings in the presence or absence of PVAT.

2. Materials and methods

2.1. Ethical statement

The study was approved by the Central Committee on Animal Experiments of The Netherlands (license AVD105002016707) and the animal welfare body of the University Medical Center Groningen (protocol 16707–01-001), which is subject to EU guidelines and laws for the use of animals in scientific research. All procedures of animal care, experimental interventions and monitoring of animal welfare were performed in accordance with such accountability. ARRIVE guidelines [15] were followed except for gender equality, as all animals were male. The reasons why we only used males were to exclude the potential effect of estrogen fluctuations on cholesterol, and that male rats show more endothelial dysfunction than female rats when challenged with a stressor [16].

2.2. Animals and study design

Male ApoE deficient rats (SD-ApoE^{tm1sage} or *ApoE*$^{-/-}$, N = 8) and their wild-type Sprague-Dawley controls (N = 8) were purchased from Sage Labs Inc. (Boyertown, Pennsylvania, USA) [17]. Animals were housed pairwise in Makrolon cages with ad libitum access to standard chow and fresh tap water during standard day/night (12 h/12 h) cycle at 21 ± 2 °C at the institutional facilities for animal studies (UMCG-CDP, Groningen, The Netherlands). At the start of the study period when rats were 8 weeks of age, high fat feeding on a high cholesterol diet (D12079B, Research Diets, New Brunswick, New Jersey, USA) was initiated.

At 59 ± 1 weeks of age, [18F]FDG PET/CT imaging was performed [13,18], and non-fasting plasma samples were obtained from the tail vein. Anesthesia was induced by inhalation of 5% isoflurane followed by 2% isoflurane mixed with oxygen for maintenance. Rats received an *iv* injection with 60 MBq of [18F]FDG and approximately 3 h later were put in a dedicated small animal PET/CT camera (D-PET, Inveon®, Siemens Preclinical Solutions, Knoxville, TN, USA). A CT scan was made followed by a 20-minute static PET scan. Animals were warmed during the procedure using heating pads set at a temperature of 38 °C and electronic temperature controllers from M2M Imaging (Cleveland, OH, USA). Subsequently, animals were terminated by exsanguination by perfusion with saline solution.

The thoracic aorta including PVAT was excised just after the arch towards the lower descending aorta and placed in ice-cold saline. From a total segment length of approximately 1.6 cm, eight rings of 2 mm length were prepared for immediate studies of vascular (endothelial) function in organ bath experiments (4 with PVAT, 4 without PVAT). After the functional measurements, one ring (with PVAT) was selected in a randomized fashion, transferred into formaldehyde and processed for immunohistochemical analysis. To validate the uniformity of selected thoracic aortic rings, internal circumference was measured in all histological images used for quantification, demonstrating no differences between *ApoE*$^{+/+}$ and *ApoE*$^{-/-}$ groups (p = 0.26, Supplementary Fig. 4A, B). Removed aortic PVAT was snap-frozen and stored at −80 °C for molecular analysis.

2.3. Blood chemistry

Upon blood collection, a small sample was used for immediate measurement of blood glucose with a portable blood glucose meter (Accu-Chek Aviva, Roche, Almere, The Netherlands), expressed in

mmol/L. The remainder of the blood samples was collected into EDTA-coated tubes for assessment of plasma total cholesterol and triglycerides, measured using commercially available kits (Roche Diagnostic, Basel, Switzerland), both expressed in mg/dL. In addition, plasma hydrogen peroxide (H_2O_2) concentrations were determined using the Amplex Red assay kit by following the manufacturer's instructions (A22188, Life technologies, Leusden, The Netherlands), and expressed in μmol/L, as an index of systemic ROS levels.

2.4. Assessment of total body fat using CT

The micro-CT scan (40 kV, 250 μA, total rotation of 360° in 360 steps and an exposure time of 350 ms) was performed with the thorax in the field of view (Supplementary Fig. 1). Reconstructed CT images were acquired from all animals and then visualized, modified, and calculated using PMOD software (PMOD Technologies LLC, Zürich, Switzerland), using the *reduce matrix tool* to limit the computational power required to process the CT images.

The Hounsfield units (HU) representing adipose tissue under these exact experimental conditions were determined as follows: (a) five images from each group were selected, (b) a region of interest (ROI) of adipose tissue was manually drawn for each image, (c) the average Hounsfield value, and standard deviation (SD), for all pixels in each ROI were noted. To exclude pixels with extreme values that might not represent adipose tissue, the mean $\pm 2 \times$ SD (95% of data-points around the average in an assumed Gaussian distribution) was selected as a threshold value of adipose tissue in each ROI. (d) Upper and lower threshold averages were calculated [−133 HU; −432 HU] and selected as the final Hounsfield interval used for subsequent adipose tissue segmentation.

To avoid artifacts in the segmentation, several adjustments were made to the raw images prior to analysis. (I) One of the most prominent artifacts, the lungs, was excluded by selecting the abdominal region as representative for the whole body, and a segment of 300 slices below the lungs was used for quantification of body fat. To quantify the exact same region for all datasets, an anatomical reference point was determined. For each dataset, a full-body image was loaded in PMOD software and segmented. The slice-number that delineated the lowest part of the lungs was set as reference. The image was re-loaded in PMOD, with the pre-processing criteria to only load the reference slice and the subsequent 300 slices. (II) The bed, on which the animal was positioned during the scan, was another artifact that was excluded. A single ROI was drawn around the bed surface, and then copied to all slices. The resulting volume of interest (VOI), constituting the whole bed volume, was then masked. (III) Eventually, adipose tissue segmentation was performed, and body fat percentage calculated from total body volume and adipose tissue volume using Hounsfield units in the range − 133 to −432.

2.5. Measurement of PVAT volume using PET

Micro PET acquisition was performed for 20 min, and the data reconstructed using OSEM3D/MAP algorithm with a voxel size of 0.39 $\times$ 0.39 $\times$ 0.80 mm and linear resolution at the center of the field-of-view of 1.2 mm. PET scans were corrected for decay, random coincidences, scatter, and attenuation. CT data were reconstructed using the Filtered Back Projection (FBP) algorithm creating images with a maximum voxel size of 0.1 $\times$ 0.1 $\times$ 0.1 mm. PMOD version 3.9 software (PMOD Technologies Ltd., Zürich, Switzerland) was used to fuse PET and CT images and to quantify PVAT volume (cm^3) and [18F]FDG uptake as Standard Uptake Volume (SUV) in PVAT.

Fused PET/CT images were used to select the diaphragm as the anatomical reference point for the analysis of PVAT (Supplementary Fig. 2). A region of interest (ROI) with a diameter of 2.4 mm was drawn around the aortic lumen in a total of 5 planes which resulted in a 3D volume of interest (VOI). The aortic region was masked. A second ROI (diameter of 6 mm) was drawn around the PVAT in the same 5 planes. Everything outside this created VOI was masked. Background noise inside the VOI was removed using a threshold of below 60 kBq/cc. Volume (cm^3) was calculated from standardized uptake values (SUV) within the VOI.

2.6. Immunohistochemistry in rat aorta and aortic PVAT

Thoracic aortas with surrounding PVAT were embedded in paraffin and 4 μm thick sections were cut on 76x26mm glass slides (Starfrost, Brunswick, Germany). Next, slides were deparaffinized using xylene and hydrated by decreasing concentrations of ethanol. Subsequently, sections were stained with hematoxylin for 10 min, washed with running tap water for 10 min, then stained with eosin for 2 min. Afterwards, the slides were dehydrated and covered. For a separate set of histological analyses on formalin-fixed, paraffin-embedded (FFPE) sections, antigens were retrieved overnight by incubation in 0.1 M Tris-HCl (pH 9.0) at 80 °C and endogenous peroxidase was blocked with 0.03% H_2O_2. Aortic sections were then incubated with mouse-anti-rat CD68 (ED1, 1:1000, MCA341R, Bio-Rad Laboratories, Veenendaal, The Netherlands), diluted in PBS enriched with 1% BSA for 60 min at room temperature followed by several washes with PBS. Subsequently, slides were incubated for 30 min at room temperature with secondary antibody (1:100, rabbit anti-mouse HRP-conjugated, P0260, Dako, Amstelveen, The Netherlands) diluted in PBS enriched with 1% BSA and 1% normal rat serum and washed several times with PBS. Afterwards, tertiary antibody (1:100 dilution, goat anti-rabbit HRP-conjugated, P0448, Dako) diluted in PBS enriched with 1% BSA and 1% normal rat serum was incubated on tissue slides for 30 min at room temperature. Peroxidase activity was visualized by applying the chromogen 3′,3′-diaminobenzidine (DAB) for 10 min and counterstained with hematoxylin for 10 min. Following dehydration with ethanol, slides were covered with mounting medium and cover glass and imaged using a digital slide scanner (Hamamatsu NanoZoomer 2.0 HT, Japan). Presence of $ED1^+$ macrophages was quantified in a blinded fashion by counting the strong positive pixels (N_{sp}) relative to the total surface (A_{tot}) using Aperio ImageScope (v12.3.3.5048, Leica Biosystems, Amsterdam, Netherlands) and dividing the two to obtain strong positivity signal N_{sp}/A_{tot} ratio.

Aortic media thickness was determined using ImageJ version 1.53c in light microscopy images by drawing a straight line across the media at 12 different points per section evenly distributed across the wall circumference, and taking the arithmetic mean per animal. Similarly to the material used in the staining of vascular lesions, the sections used for the measurement of media thickness were prepared from the same rings taken at random from the descending thoracic aorta. Intima and media surface were measured using ImageJ by subtracting total lumen surface from lumen plus intima surface and by subtracting total lumen surface from lumen plus intima plus media surface, respectively. The measured values were used to calculate the ratio between the intima and media surfaces.

The marker of proliferation Ki67 was stained in deparaffinized FFPE sections of rat PVAT, and human placenta and rat kidney were used as positive controls. Epitopes were retrieved by heating in the microwave for 15 min at 300 W in 0.1 M Tris/HCl buffer pH 9. After washing with PBS, endogenous peroxidases were blocked with 0.03% H_2O_2 for 30 min. The sections were incubated with Anti-Ki67 (1:250 dilution, clone MIB-1, M7240, Dako) with 1% rat serum for 60 min. After three subsequent washes with PBS each 5 min long, sections were incubated for 60 min with a secondary rabbit anti-mouse antibody conjugated with HRP (1:100 dilution, P0260, Dako) enriched with 1% rat serum. After another three washes with PBS, signal was enhanced with a tertiary HRP-conjugated goat anti-rabbit antibody (1:100 dilution, P0448, Dako) enriched with 1% rat serum. The protocol was concluded using DAB as chromogen and hematoxylin counterstain in the same fashion as the staining of ED1 described above.

2.7. Endothelial glycocalyx staining

To demonstrate the presence of the endothelium in aortic rings, FFPE sections of the aorta were stained with fluorescein-conjugated agglutinins from tomato (*Lycopersicon esculentum*, LEA-FITC, 50 μg/mL, FL-1171, Vector Laboratories, Burlingame, California, USA) and wheat (*Wheat germ*, WGA-FITC, 50 μg/mL, FL-1021, Vector Laboratories). Aortic sections were deparaffinized and re-hydrated as described above, and antigen-retrieval was performed using 10 mM citrate pH 6 by boiling in the microwave for 5 min. After cooling to room temperature, sections were washed twice with PBS and encircled using a fatty pen. Each glass slide contained two sections, of which one was incubated for 1 h either with LEA-FITC or WGA-FITC, and the other section was incubated with PBS as control. Subsequently, glass slides were washed three times with PBS, and mounted using Vectashield with DAPI (H-1200-10, Vector Laboratories). Images were taken using a Leica digital microscope camera (DFC3000 G) mounted on a fluorescent microscope (DM2000 LED) with a 20× magnification.

2.8. mRNA quantification in PVAT using RT-qPCR

Aortic PVAT was studied for mRNA expression of cyclooxygenase-2 (COX2), IL-1β, IL-6, CCL2 (MCP-1), CD68 as indices of inflammation and adiponectin (ADIPOQ) for anti-inflammation. In addition, eNOS and UCP-1 expression were studied in PVAT, and UCP-1 expression was additionally studied in abdominal visceral adipose tissue. Samples of snap-frozen PVAT were homogenized on ice using an electronic pestle and RNA was isolated using TRIzol reagent according to manufacturer's instructions (Thermo Fisher, Blijswijk, the Netherlands). The concentration of RNA was measured spectrophotometrically at 260 nm and 1 μg RNA was reversely transcribed into cDNA. Quantitative real-time PCR was performed using AbsoluteTM QPCR SYBR® Green ROX Mix (Westburg, Leusden, Netherlands), 400 nM of primer and 2 μL template DNA in a total volume of 10 μL. The reaction was performed at 95 °C for 15 min followed by 40 cycles of denaturation at 95 °C for 15 s and annealing or extending at 60 °C for 1 min. Primers were received from manufacturer in 100 μM desalted TE solution (Sigma-Aldrich, Zwijndrecht, The Netherlands); primer sequences are showcased in Supplementary Table 1. Data were acquired in Bio-Rad CFX Manager version 3.0 (Bio-Rad Laboratories Inc., Hercules, CA, United States), and normalized in R version 4.1.0 using the $2^{-\Delta\Delta Ct}$ method as described before [19], by using the *Hprt1* housekeeping gene and $ApoE^{+/+}$ controls as reference group (Supplementary Fig. 3).

2.9. Endothelial function measurements in isolated rat aorta rings

The freshly obtained aorta was transferred into normal Krebs solution of the following composition (mmol/L): NaCl, 120.4; KCl, 5.9; $CaCl_2$, 2.5; $MgCl_2$, 1.2; NaH_2PO_4, 1.2; glucose, 11.5; $NaHCO_3$, 25.0. The aorta was carefully cut into multiple 2 mm rings, either with or without PVAT (Supplementary Fig. 4C, D) and mounted between two stirrups in organ baths filled with 15 mL of Krebs solution continuously aerated with 95% O_2 and 5% CO_2 and containing 10 μmol/L indomethacin (I7378 Sigma-Aldrich), a non-selective inhibitor of COX, to avoid potential interference of vasoactive prostanoids. One stirrup was anchored inside the organ bath and the other connected to a displacement transducer to determine isotonic changes (in μm), as described previously [20]. Rings were subjected to 14 mN pressure and allowed to stabilize for 60 min at 37 °C before they were checked for viability by evoking a contraction with 60 mmol/L KCl (twice with intermediate washes).

After washout and renewed stabilization, rings were pre-constricted with 1 μmol/L phenylephrine (PE), given time to stabilize the response, and then stimulated by cumulative additions of acetylcholine (ACh, 3 nmol/L – 100 μmol/L; A6625, Sigma-Aldrich) to assess endothelium-dependent relaxation (EDR). All drugs were given in a cumulative fashion and all concentration ranges represent final bath concentrations. After assessment of the effect of the highest concentration of ACh, a washout and renewed stabilization period followed. In a second phase, rings were first pre-incubated (20 min) with 100 μmol/L N^G-monomethyl-L-arginine, (L-NMMA, Sigma-Aldrich Zwijndrecht, The Netherlands), an inhibitor of eNOS, before the above PE-ACh protocol for EDR was repeated. To assess the efficacy of the vascular smooth muscle cells to respond to exogenous NO, a single high dose of sodium nitroprusside (SNP, 100 μM) was administered after the last ACh concentration. To present data, contractile responses to KCl and PE are shown in μm displacement, while relaxation responses to ACh and SNP are expressed as a percentage of PE pre-constriction, with PE-pre-constriction set to 0%.

2.10. Quantification of iNOS in aortic PVAT using SDS-page immunoblotting

Isolated aortic PVAT tissue was homogenized in ice-cold RIPA solution (Igepal ca-630, sodium deoxycholate and 20% sodium dodecyl sulfate (SDS) in PBS) enriched with protease inhibitor cocktail (11836170001, Roche Diagnostics, Almere, The Netherlands), sodium orthovanadate and β-mercaptoethanol. Total protein concentration was determined in the separated water phase using DC Protein assay (5000116, Bio-Rad Laboratories, Veenendaal, The Netherlands) and 25 μg protein in 25 μL per sample was loaded onto a commercial gel (4568093, Bio-Rad Laboratories) in preparation of iNOS detection, and 70 μg protein in 20 μL per sample for eNOS. Proteins were separated by electrophoresis and transferred onto a nitrocellulose membrane using Trans-Blot Turbo System (1620115 and 10026938 respectively, Bio-Rad Laboratories). Free nitrocellulose sites were blocked with 5% skim milk (70166, Sigma-Aldrich, Zwijndrecht, The Netherlands) for 20 min and membranes were incubated overnight at 4 °C with anti-iNOS/NOS2 antibody (1:1000 dilution, 610333, BD Biosciences, San Jose, CA, USA) in 3% BSA. After three subsequent washes with TBST, membranes were incubated with a secondary antibody Rabbit Anti-Mouse Ig/HRP (1:2000, P0260, Dako) at RT for 2 h. Chemiluminescent signal was produced using Western Lightning Ultra (NEL112001EA, Perkin Elmer International, Groningen, The Netherlands). Chemiluminescent iNOS signal was normalized to total lane protein volume using the standard BioRad Stain-Free TGX blot technology [21–25]. Relative protein expression was normalized to a standard sample which was included in all blots. Technical duplicates were averaged before summary statistics were performed on relative expression per individual animal.

2.11. Data analysis and statistics

GraphPad Prism version 8.4.2. was used for data analysis. Data points in tables and figures are expressed as mean ± SEM. Statistical inference was performed using the Mann-Whitney *t*-test unless otherwise specified, with p-values represented by * < 0.05, ** < 0.01, *** < 0.001. Inference of the mean parameters was performed as comparison between $ApoE^{-/-}$ and $ApoE^{+/+}$ groups. Means of individual data points from cumulative dose-response curves were compared between groups by repeated unpaired *t*-tests adjusted for multiple comparisons using the Holm-Sidak method.

3. Results

3.1. Animal characteristics

At the start of the study at the age of 8 weeks, body weight did not differ between $ApoE^{+/+}$ and $ApoE^{-/-}$ groups (362 ± 14 g vs 361 ± 26 g, respectively; p = NS). Also, at the end of the main study period of 51 weeks, during which both groups received a high-fat, high-cholesterol diet (HFD), body weight in $ApoE^{-/-}$ animals was not different from $ApoE^{+/+}$ controls, and neither was the percentage of total body fat (Table 1). This was despite a clear difference between both groups in the

Table 1
Animal characteristics of 59 weeks old rats after 51 weeks of a high-fat high-cholesterol diet.

	ApoE$^{+/+}$ (n = 8)	*ApoE*$^{-/-}$ (n = 7)
Body weight (g)	759 ± 24	720 ± 30
Blood glucose (mmol/L)	6.55 ± 0.50	5.89 ± 0.53
Plasma cholesterol (mg/dL)	162.2 ± 13.7	1704.8 ± 211.2*
Plasma triglycerides (mg/dL)	275.6 ± 40.5	842.0 ± 236.0*
Plasma H_2O_2 (μmol/L)	18.64 ± 3.90	30.42 ± 5.11
Body fat (% volume)	40.4 ± 1.2	40.8 ± 0.8
Thoracic aortic PVAT volume (cm^3)	0.26 ± 0.08	0.62 ± 0.03**
PVAT [18F]FDG uptake (SUV max)	10.19 ± 2.27	29.56 ± 4.66**

Data are mean ± SEM. * indicate $p < 0.05$, ** indicate $p < 0.01$.

development of hyperlipidemia over time, demonstrating markedly increased blood plasma levels of cholesterol and triglycerides in *ApoE*$^{-/-}$ rats (Table 1). Nevertheless, glucose levels were similar in both groups and within the normoglycemic range [26], suggesting no major abnormalities in systemic glycemic control. Plasma H_2O_2 levels, representative of systemic oxidative stress, were 1.5 times higher in *ApoE*$^{-/-}$ rats as compared to *ApoE*$^{+/+}$ controls ($p = 0.092$, Table 1). Interestingly, unlike the percentage of total body fat, which was comparable in both groups, *ApoE*$^{-/-}$ rats harbored significantly larger amounts of PVAT than *ApoE*$^{+/+}$ rats, as measured by combined PET/CT (Table 1). In addition, PVAT infiltration was quantified by the uptake of [18F]FDG by PET imaging, as previous reports showed this marker to be mainly taken up by tissue macrophages [11–14]. The thoracic PVAT of *ApoE*$^{-/-}$ rats showed a significantly higher PET signal than the PVAT of *ApoE*$^{+/+}$ controls.

3.2. Development of pre-atherosclerotic lesions in the thoracic aorta of aged *ApoE*$^{-/-}$ rats

Importantly, atherosclerosis was not manifested by advanced subintimal plaque formation, but rather by abluminal cell adhesion in light microscopy images of paraffin-embedded hematoxylin-stained thoracic aorta (Fig. 1A, B). In addition, adherent deposits in *ApoE*$^{-/-}$ thoracic aortas was observable on a macroscopic level when handling ring preparations (Supplementary Fig. 4C, D). Immune cell presence was revealed by staining of FFPE sections of thoracic aorta using the marker ED1 [27]. While ED1 signal was absent in the aortic intima of *ApoE*$^{+/+}$ rats, it was profound in the intima of ApoE deficient animals (Fig. 1A, B, C). Moreover, monocytes/macrophages were evident in the aortic PVAT and were significantly more abundant in *ApoE*$^{-/-}$ animals than in *ApoE*$^{+/+}$ controls (Fig. 1A, B, D). To investigate whether ED1 positive cells were present in PVAT as a result of proliferation or infiltration, we performed an immunohistochemical staining of the marker of proliferation Ki67, and found that it was completely absent in PVAT of both groups (Supplementary Fig. 5). Since atherosclerosis is often accompanied by aortic remodeling [28], we measured the thickness of the aortic media in hematoxylin-stained sections (Fig. 2A, B, C), as well as the ratio between surfaces of the intima and media (Fig. 2D). As expected, both parameters were significantly increased in *ApoE*$^{-/-}$ rats compared to *ApoE*$^{+/+}$ (Fig. 2C, D).

3.3. Perivascular adipose tissue has a pro-inflammatory phenotype in *ApoE*$^{-/-}$ rats

Given the excess ED1 and [18F]FDG signals, we subsequently explored PVAT inflammation in more detail. Transcription of the

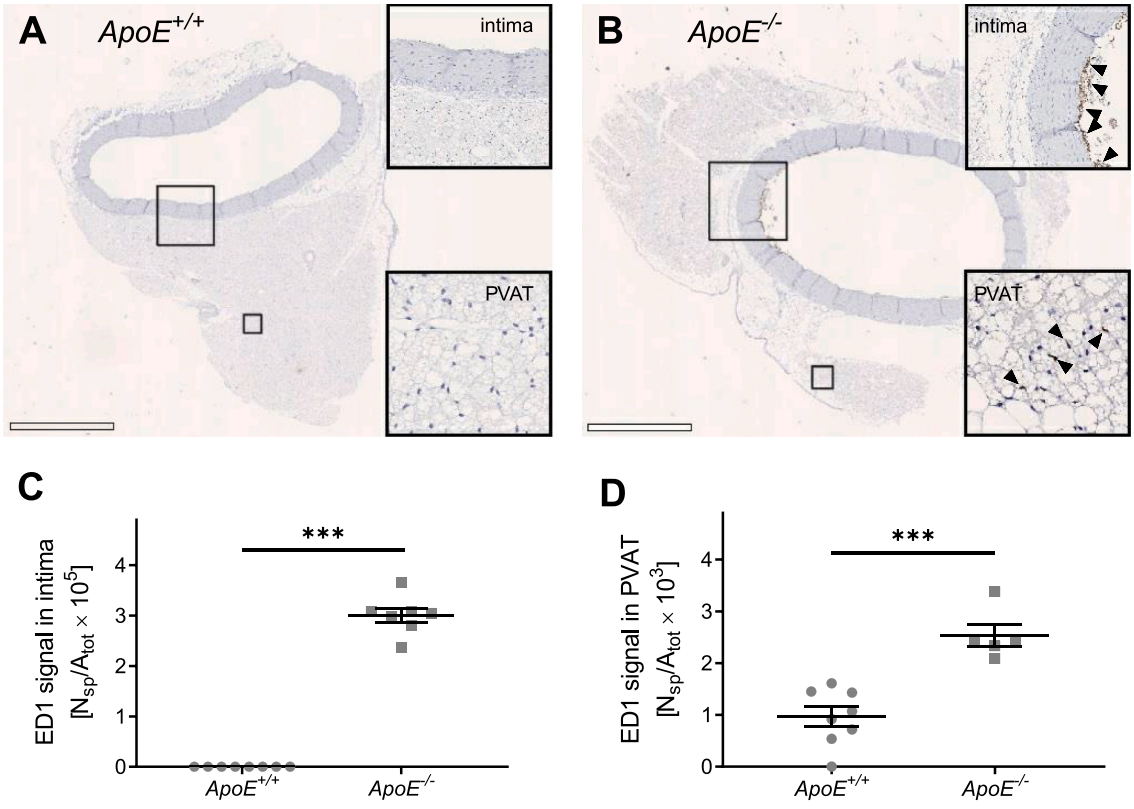

Fig. 1. Development of early atherosclerosis in thoracic aortic intima and PVAT. (A) Representative light microscopy images of ED1 staining of macrophages in aorta from an ApoE$^{+/+}$ control, and (B) from ApoE$^{-/-}$ rat. Scale bars represent 1 mm, and insets represent a magnification of highlighted sections of thoracic aortic wall intima and PVAT. Black arrow heads point to locations with positive ED1 signal. (C) Quantification of ED1 staining signal in aortic intima as the ratio of strong positive pixels (N_{sp}) and the total surface (A_{tot}), and (D) quantification of ED1 positive signal in aortic PVAT. Bars represent mean ± SEM, with N = 8 ApoE$^{+/+}$ and N = 7 ApoE$^{-/-}$ rats in (C), and N = 8 ApoE$^{+/+}$ and N = 5 ApoE$^{-/-}$ rats in (D). ** indicate $p < 0.01$ and *** indicate $p < 0.001$ calculated using the Mann-Whitney test.

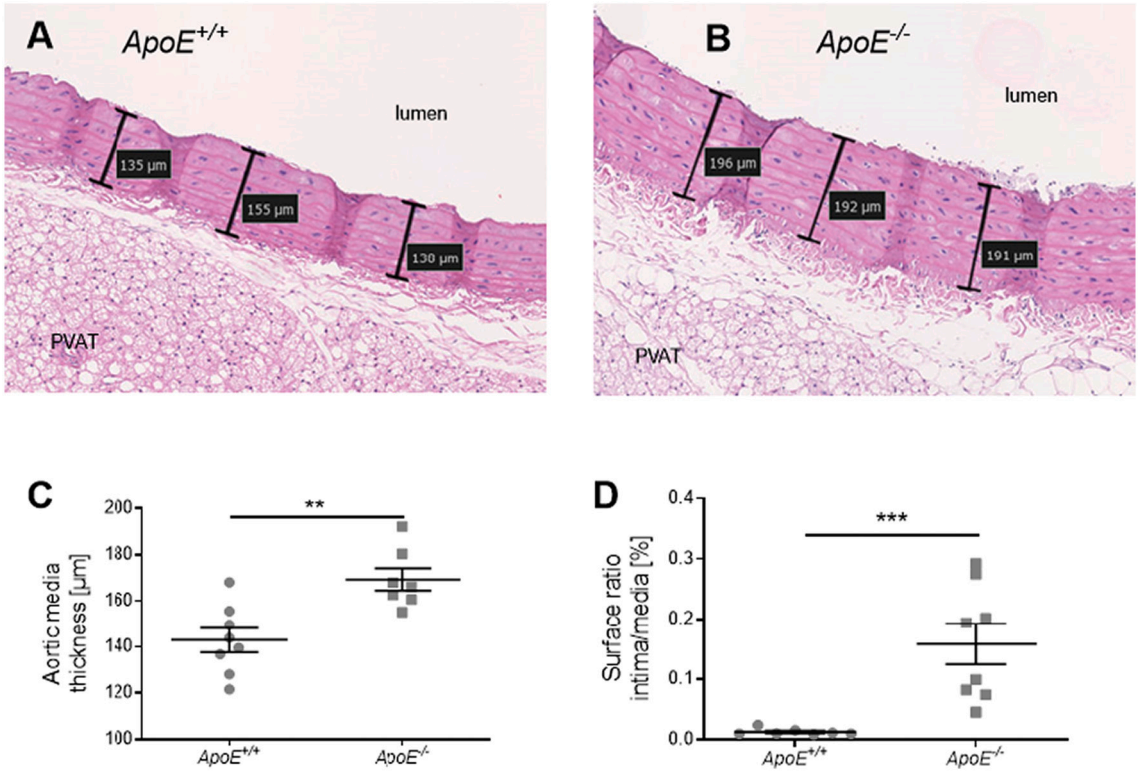

Fig. 2. Thoracic aortic wall remodeling in ApoE$^{-/-}$ rats. (A) Representative light microscopy images of hematoxylin/eosin staining of aorta from ApoE$^{+/+}$ control, and (B) of an ApoE$^{-/-}$ rat. (C) Quantification of aortic media thickness, (D) ratio between the surfaces of aortic intima and media. Bars represent mean ± SEM, with N = 8 ApoE$^{+/+}$ and N = 7 ApoE$^{-/-}$ rats in (C), and N = 7 ApoE$^{+/+}$ and N = 8 ApoE$^{-/-}$ rats in (D), ** and *** indicate $p < 0.01$ and $p < 0.001$ respectively, calculated using the Mann-Whitney test.

macrophage marker CD68 [29] was significantly increased in PVAT of *ApoE*$^{-/-}$ rats compared to controls (Fig. 3A), confirming infiltration, while the mRNA of the macrophage recruitment marker MCP-1 [30] remained unchanged (Fig. 3A).

Considering that NO is also a pro-inflammatory mediator capable of recruiting monocytes [31], we measured the protein expression of iNOS and found a significant increase in PVAT of *ApoE*$^{-/-}$ animals (Fig. 3B). The inflammatory cytokine and activator of iNOS, IL-1β[31] was significantly up-regulated on the mRNA level in the PVAT of *ApoE*$^{-/-}$ animals, while IL-6, adiponectin (*ADIPOQ*) and cyclooxygenase 2 (COX2) were unchanged (Fig. 3A).

As whitening of PVAT is expected in inflammatory conditions [32], the mRNA expression of the marker of browning UCP-1 was measured. Even though one *ApoE*$^{-/-}$ rat demonstrated high UCP-1 expression, the average expression was not different between *ApoE*$^{-/-}$ and *ApoE*$^{+/+}$ rats (Supplementary Fig. 6). When compared with abdominal visceral adipose tissue that represents a generally white adipose tissue [32], the mRNA expression of UCP-1 was similar in PVAT (Supplementary Fig. 6).

3.4. PVAT rescues endothelial dysfunction in ApoE$^{-/-}$ rat aorta

As endothelial dysfunction is typically present in atherosclerotic arteries, the functional responses of rat aortas were assessed in isotonic displacement studies. In thoracic aortic rings with PVAT removed, maximal ACh-induced relaxation was already considerably low in *ApoE*$^{+/+}$ rats (40% of pre-constriction) and was significantly impaired even further in *ApoE*$^{-/-}$ animals (15% of pre-constriction, $p = 0.012$, PVAT- in Fig. 4A and C). To make a clear distinction between endothelial damage and dysfunction, the presence of the endothelial layer was verified by staining of the glycocalyx in FFPE sections of aortas. Using a combination of tomato and wheat lectins conjugated with FITC, and DAPI staining of the nucleus, we found that the aortic endothelium was intact in *ApoE*$^{+/+}$ and *ApoE*$^{-/-}$ rats alike (Supplementary Fig. 7). To investigate the involvement of PVAT in EDR, responses were also determined simultaneously in rings with PVAT left intact. In *ApoE*$^{+/+}$ rats, relaxation induced by ACh was identical in PVAT- and PVAT+ preparations (Fig. 4A). In contrast, presence of PVAT markedly enhanced the ACh-induced relaxation in *ApoE*$^{-/-}$ animals (Fig. 4C), even surpassing relaxation of *ApoE*$^{+/+}$ rings with PVAT (*ApoE*$^{-/-}$ 65%, *ApoE*$^{+/+}$ 42%, $p = 0.012$, Fig. 4A and C: PVAT+). This dissimilarity between effects of PVAT on EDR in *ApoE*$^{+/+}$ and *ApoE*$^{-/-}$ rats was not due to differences in pre-constriction levels, because contractile responses to 60 mM KCl and 1 µM PE were comparable (Supplementary Table 2). When repeated in the presence of L-NMMA, ACh induced relaxations were fully abolished in all rings, demonstrating that aortic relaxation was exclusively mediated by NO (Fig. 4B, D). L-NMMA also enhanced 1 µM PE pre-constriction levels, yet this was similar in both groups (Supplementary Table 2). Moreover, endothelium-independent relaxation to a high dose of SNP resulted in similar responsiveness of the vascular smooth muscle to exogenous NO (Supplementary Table 2). Given that NO acted as a central mediator of endothelium- and PVAT-dependent vasorelaxation in this model, eNOS mRNA was quantified in PVAT and was found significantly upregulated in *ApoE*$^{-/-}$ rats (Fig. 4E).

4. Discussion

In the present study, we employed a model of early atherosclerosis induced by a combination of genetic knockout of ApoE and HFD in rats to elucidate the mechanism by which PVAT contributes to preservation of arterial relaxation. *ApoE*$^{-/-}$ rats were diet- and age-matched to *ApoE*$^{+/+}$ Sprague-Dawley controls and both groups received a HFD for 51 weeks. *ApoE*$^{-/-}$ rats exhibited hyperlipidemia and atherogenesis in the aorta by the means of macrophage abundance and inflammation in

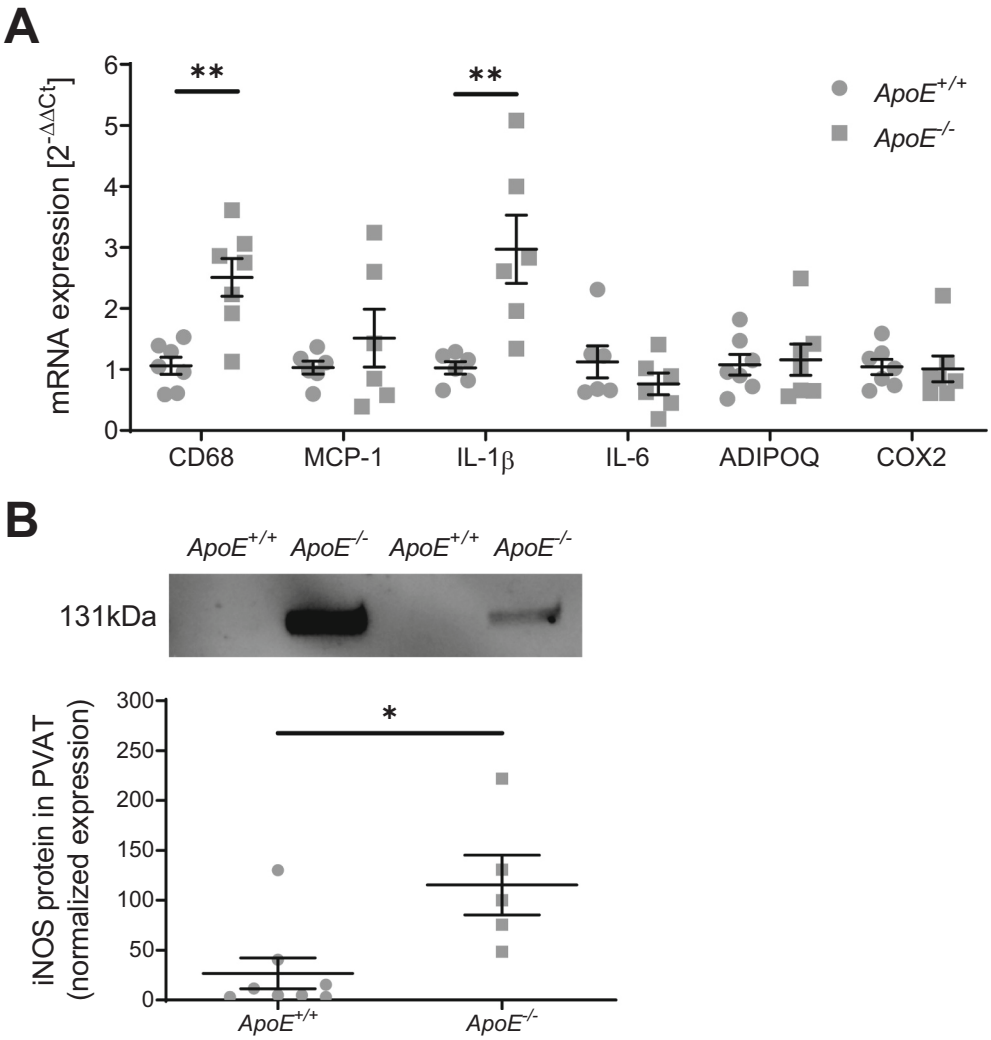

Fig. 3. Inflammatory markers in thoracic aortic PVAT ApoE$^{-/-}$ and ApoE$^{+/+}$ control rats. (A) Inflammatory marker mRNA expression, and (B) iNOS protein expression in thoracic aortic PVAT. Bars are expressed as mean ± SEM, with N = 6–8 ApoE$^{+/+}$ and N = 6–7 ApoE$^{-/-}$ rats in (A), and N = 8 ApoE$^{+/+}$ and N = 5 ApoE$^{-/-}$ rats in (B). * and ** indicate $p < 0.05$, $p < 0.01$ calculated using the Mann-Whitney test, respectively.

the aortic intima, media thickening and substantial endothelial dysfunction. Interestingly, the PVAT of *ApoE*$^{-/-}$ animals demonstrated an inflammatory phenotype yet boosted acetylcholine-mediated aortic relaxation in an NO-dependent manner.

Although mouse genetic models of hyperlipidemia such as the *LDLr*$^{-/-}$ or *ApoE*$^{-/-}$ are employed commonly, the rat *ApoE*$^{-/-}$ model has become increasingly popular in the study of endothelial dysfunction and plaque imaging in atherosclerosis [4,16,33,34]. The rat population in our study was limited to only males, in order to exclude potential effects of estrogen on plasma cholesterol. With regards to endothelial relaxation, it is possible that differences exist between male and female rats in this model [16]. The phenotype in our model corresponded with current literature, and was characterized by hypercholesterolemia [2] and pre-atherosclerotic lesion development recognizable ex vivo by the naked eye.

As expected, PVAT of *ApoE*$^{-/-}$ animals in our study was occupied by macrophages as supported by increased ED1 staining, [18F]FDG uptake and CD68 mRNA expression. Similar findings were previously observed in mice that were fed a HFD and in mice with PPAR-γ deficiency-associated atherosclerosis [35,36]. Moreover, we observed that increased macrophage presence was accompanied by overexpression of iNOS protein in aortic PVAT. Recently, it was demonstrated that iNOS expressed in macrophages promoted inflammation by further recruiting monocytes, supporting their differentiation into macrophages and formation of foam cells [31]. In addition, macrophages were previously found to proliferate in adipose tissue of obese mice based on the marker Ki67 [37], while in our study Ki67 was not detectable in PVAT. This led us to hypothesize that increased monocyte infiltration into PVAT and their differentiation into macrophages in *ApoE*$^{-/-}$ rats was mediated largely by NO originating from iNOS activity. In support of increased NO-mediated monocyte infiltration in *ApoE*$^{-/-}$ rats, the expression of the monocyte chemoattractant protein, MCP-1, was unaltered in *ApoE*$^{-/-}$ PVAT in our study. Furthermore, expression of the pro-inflammatory cytokine IL-1β, which is widely accepted as activator of iNOS, was strongly increased in PVAT of *ApoE*$^{-/-}$ rats. Finally, considering that markers of inflammation were measured after normalization for content of mRNA or protein, their true levels and effects in vivo are likely multiplied when accounting for the increased volume of PVAT measured with PET imaging.

Surprisingly, the mRNA expression of the adipocytokine adiponectin was unchanged in *ApoE*$^{-/-}$ PVAT, despite evident development of early atherosclerotic lesions and vascular inflammation. Previously, it was reported that healthy PVAT confers atheroprotective effects by an increased secretion of adiponectin, which in turn promotes the phosphorylation of eNOS via AMPK and production of NO. [6,38,39] Unchanged mRNA adiponectin expression may have resulted from adaptive

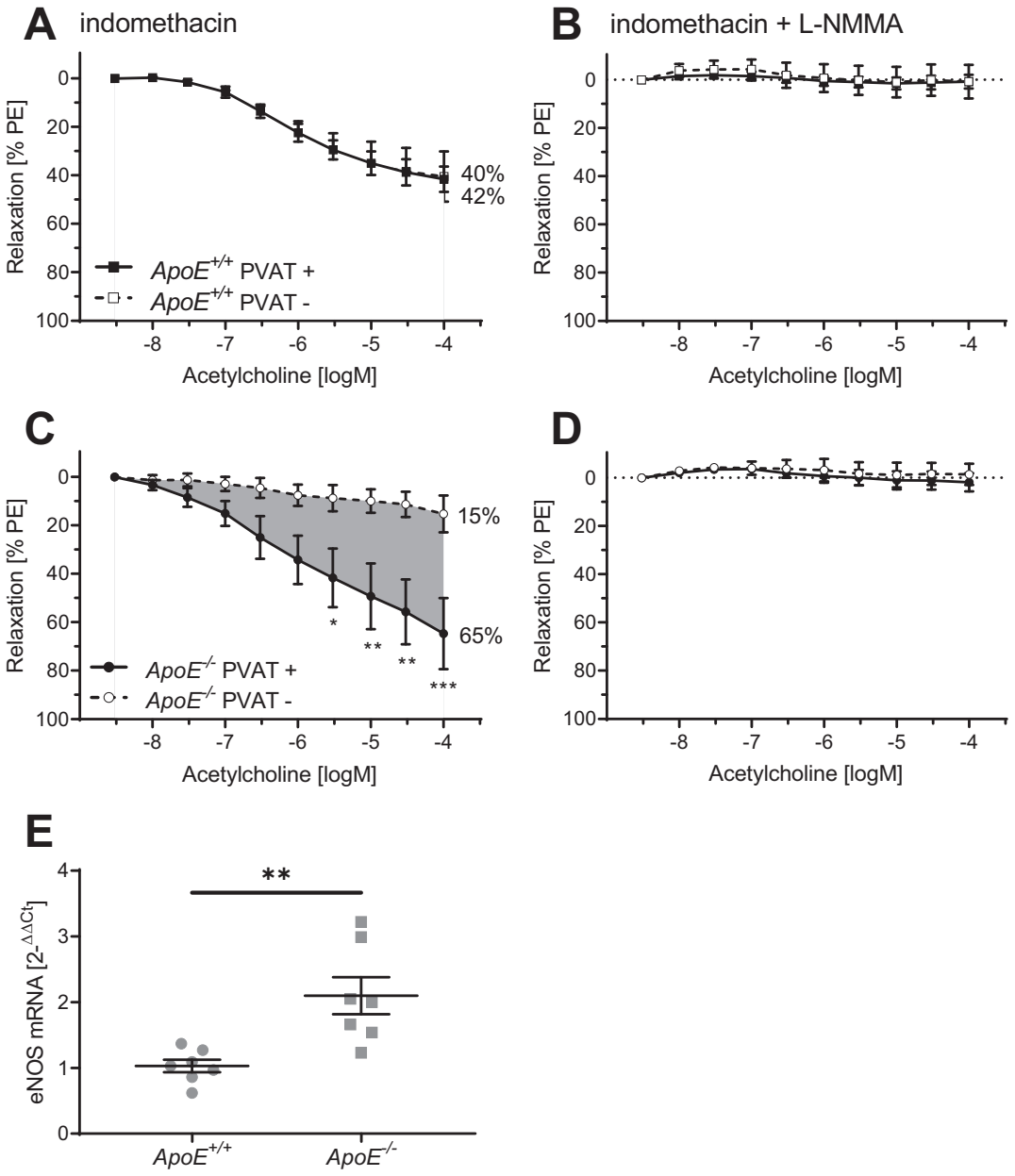

Fig. 4. Endothelium-dependent relaxation of the rat thoracic aorta with (+) and without (−) PVAT. Acetylcholine-induced relaxation response of aortic rings from (A) wild-type or (B) ApoE−/− animals with PVAT (solid line) and without PVAT (dashed line) in the presence of indomethacin. Relaxation responses of (C) wild-type and (D) ApoE deficient aortic rings in the presence of indomethacin and L-NMMA. (E) mRNA expression of eNOS in thoracic aortic PVAT. Data points in (A-D) are expressed as mean ± SEM, with N = 5–8 rats per group. In E), bars represent mean ± SEM, with N = 7 rats per group. *, ** and *** indicate $p < 0.05$, $p < 0.01$ and $p < 0.001$, respectively. Means of individual data points in (A-D) were compared using multiple unpaired *t*-tests with the Holm-Sidak correction for multiple comparisons, and sample means in E) were compared using the Mann-Whitney test.

mechanisms that may have occurred during the 51 weeks of HFD and considering that in our study the age of rats at assessment was 59 weeks. Although mRNA expression levels lend indication of the expression of adiponectin in PVAT in hyperlipidaemia and inflammation, the true function of the protein may be dependent on oligomerization, especially when considering that a shift between monomeric and oligomeric species can differentially activate AMPK [40].

As expected, our 59 weeks-old control SD rats displayed endothelial dysfunction in terms of low acetylcholine-induced, NO-mediated EDR (40%), in line with previous observations in 52-week old wild-type mice (40%) [41] and in rodents on HFD feeding [42]. In addition, *ApoE*$^{-/-}$ and HFD further impaired relaxation, with only 15% relaxation remaining. The extent of endothelial dysfunction was rather severe in comparison to 16-week old *ApoE*$^{-/-}$ rats in which EDR was reported to be as high as 43% of PE pre-constriction [43].

Importantly, the impairment of EDR was present despite an intact endothelium and was only observed in thoracic aortic segments without PVAT. Presence of PVAT strongly enhanced acetylcholine-induced relaxation in *ApoE*$^{-/-}$ aortas, whereas this effect was absent in *ApoE*$^{+/+}$ controls. This finding extends the previously reported rescue of aortic endothelial function by PVAT in atherosclerosis in adult *LDLr*$^{-/-}$ mice [4], by demonstrating a similar, albeit stronger effect of PVAT in aged rats with early-stage atherosclerosis in the current study. In another study, PVAT enhanced EDR in mesenteric arteries from rats with metabolic syndrome, however this effect was only observed at the age of 17 to 20 weeks and disappeared at 23 weeks [44]. Unfortunately, this

report did not include the effect of PVAT on EDR in control rats. Since in the current cohort we do not discriminate between the effects of diet and age, we cannot infer whether these factors influence the rescue of relaxation by PVAT in *ApoE*$^{-/-}$ rats. Nevertheless, *ApoE*$^{-/-}$ aortas clearly demonstrated a rescue of endothelial dysfunction by PVAT.

Furthermore, the PVAT-mediated rescue of EDR in *ApoE*$^{-/-}$ was entirely mediated by NO, given that it was fully blocked by L-NMMA. Consistent with our finding, it was demonstrated before that PVAT of mouse aorta expressed eNOS and produced NO. [4,45,46] In our study, this phenomenon was supported by evidence of increased eNOS transcription in *ApoE*$^{-/-}$ PVAT. As a limitation, the finding was not confirmed on protein level due to technical difficulties despite extensive optimization attempts for antibodies against total-eNOS and phospho-eNOS. Nevertheless, based on aortic relaxation experiments we argue that enhanced NO contribution by PVAT originates from eNOS and not iNOS, since only eNOS is momentarily inducible by acetylcholine stimulation of muscarinic receptors and calcium flux, while iNOS is inducible on the transcription level by inflammatory cytokines [47]. Arguably, basal NO activity originating from iNOS in PVAT did not play a role in vasomotor studies, as pre-constriction levels of KCl and PE were not decreased in rings with PVAT.

We also excluded the possibility of impaired NO responsivity of the vascular smooth muscle in NO-mediated vasorelaxation based on a single high dose of SNP which produced maximal relaxation in aortas with and without PVAT from both *ApoE*$^{-/-}$ and *ApoE*$^{+/+}$ rats. These results matched previous measurements of SNP responses in LDLr deficient mice [4].

Further we observed that prostaglandins did not exhibit a significant role in smooth muscle relaxation mediated by the endothelium or PVAT, as blocking COX-1 and COX-2 by indomethacin did not affect constrictions to single-dose PE. Moreover, addition of L-NMMA to indomethacin treated rings did not affect PE constriction of aortas with and without PVAT, supporting similar basal NO release in both groups, despite elevated expression of eNOS and iNOS in *ApoE*$^{-/-}$ PVAT. Lastly, the complete loss of all ACh-induced relaxation after combined pre-incubation with L-NMMA and indomethacin demonstrated the lack of endothelium-derived hyperpolarizing factor (EDHF) in both *ApoE*$^{-/-}$ and *ApoE*$^{+/+}$ aortas. Although we did not perform studies in endothelium-denuded arteries, the effect of PVAT specifically on the endothelium in atherosclerosis is worth investigating in future studies.

Admittedly, the aorta serves as a conduit artery and has low impact on the regulation of systemic blood pressure. Nevertheless, the aorta is routinely used as a model for endothelial dysfunction which is considered one of the first symptoms in the development of atherosclerosis [51]. Moreover, arteries of a larger caliber typically harbor larger amounts of PVAT compared to small peripheral resistance arteries such as the mesenteric. In addition, atherosclerosis typically develops in large-diameter arteries, altogether supporting the choice of the aorta as a relevant model in the present study.

When considering human atherosclerosis, the carotid artery, coronary artery, and abdominal aorta are the main sites affected by plaque development [14,29,48], while thoracic aortic atherosclerosis was found to be a predictor of coronary artery disease [49]. The thoracic aorta and abdominal aorta have anatomical and functional differences that may be involved in susceptibility to atherosclerosis. The phenotype of abdominal aortic PVAT resembles white adipose tissue with a higher pro-inflammatory tendency than thoracic aortic PVAT, which has a phenotype that resembles brown adipose tissue [50]. While not investigated in our study, it would be of interest to investigate whether the effects of thoracic aortic PVAT on relaxation in *ApoE*$^{-/-}$ rats are also present in the abdominal aorta. With regards to adipose tissue phenotype, our results indicated that the level of mRNA expression of UCP-1 in PVAT was not different between *ApoE*$^{-/-}$ and *ApoE*$^{+/+}$ rats, suggesting that thoracic PVAT in *ApoE*$^{-/-}$ rats did not undergo changes in brown adipose tissue phenotype.

Hyperlipidemic *ApoE*$^{-/-}$ rats demonstrated a trend towards an increased plasma ROS load represented by H_2O_2, although the differences in means were not statistically significant. Still, chronic exposure to elevated ROS may exacerbate the progression of endothelial dysfunction and atherosclerosis [52]. On the other hand, H_2O_2 has been recently shown to emit vasoprotective effects. Specifically, when released from BAT via Nox4, H_2O_2 induced GMP-dependent PKG, decreasing vascular contractility [53]. Considering that aortas in our organ baths were no longer exposed to H_2O_2 from systemic circulation and that PVAT generally has a phenotype mildly resembling that of BAT, it is conceivable that the release of PVAT-derived H_2O_2 may play a functional role in regulating aortic homeostasis in atherosclerosis. As of now, we do not know whether BAT or PVAT contributed significantly to systemic pools of H_2O_2.

Taken together, our study builds upon existing data by using aged *ApoE*$^{-/-}$ rats in combination with HFD feeding as a model of early atherosclerosis to demonstrate a novel mechanism by which PVAT rescues endothelial dysfunction. We propose that NO released by PVAT after cholinergic activation of eNOS with acetylcholine and directly acting on VSMCs to rescue arterial relaxation is the most plausible mechanism explaining our present findings. Considering that this phenomenon was captured in aged *ApoE*$^{-/-}$ rats with severe endothelial dysfunction, it might well be present in the elderly and contributing to longevity by regulating blood pressure and preventing further exacerbation of complications associated with atherosclerosis.

Financial support

D.N. was financially supported by a Abel Tasman PhD scholarship by the Graduate School of Medical Sciences, University of Groningen, University Medical Center Groningen and by Life Sciences and Health - Topconsortium voor Kennis en Innovatie (Stichting LSH-TKI): PPP project-2019-017.

Declaration of Competing Interest

The authors declare no conflict of interest.

Acknowledgements

The authors wish to thank Michelle Luxwolda for technical assistance in vascular organ bath studies, Sebastian Kristensen for PET data processing, Dr. Guido Krenning for kindly gifting tomato and wheat lectins, and Marian Bulthuis for technical assistance with staining using lectins. Graphical abstract was created with BioRender.com.

Appendix A. Supplementary data

Supplementary data to this article can be found online at https://doi.org/10.1016/j.vph.2021.106945.

References

[1] H. Wang, et al., Global, regional, and national life expectancy, all-cause mortality, and cause-specific mortality for 249 causes of death, 1980–2015: a systematic analysis for the global burden of disease study 2015, Lancet 388 (2016) 1459–1544.
[2] B. Emini Veseli, et al., Animal models of atherosclerosis, Eur. J. Pharmacol. 816 (2017) 3–13.
[3] J.G. Lee, et al., Knockout rat models mimicking human atherosclerosis created by Cpf1-mediated gene targeting, Sci. Rep. 9 (2019).
[4] N. Baltieri, D.M. Guizoni, J.A. Victorio, A.P. Davel, Protective role of perivascular adipose tissue in endothelial dysfunction and insulin-induced vasodilatation of hypercholesterolemic LDL receptor-deficient mice, Front. Physiol. 9 (2018).
[5] M.S. Fernández-Alfonso, et al., Role of PVAT in coronary atherosclerosis and vein graft patency: friend or foe?: dual role of PVAT, Br. J. Pharmacol. 174 (2017) 3561–3572.
[6] R. Aghamohammadzadeh, et al., Perivascular adipose tissue from human systemic and coronary vessels: the emergence of a new pharmacotherapeutic target: signals from PVAT, Br. J. Pharmacol. 165 (2012) 670–682.

[7] M. Reijrink, et al., Visceral adipose tissue volume is associated with premature atherosclerosis in early type 2 diabetes mellitus independent of traditional risk factors, Atherosclerosis 290 (2019) 87–93.

[8] M. Reijrink, et al., [18F]FDG uptake in adipose tissue is not related to inflammation in type 2 diabetes mellitus, Mol. Imaging Biol. (2020), https://doi.org/10.1007/s11307-020-01538-0.

[9] S. Hildebrand, J. Stümer, A. Pfeifer, PVAT and its relation to Brown, beige, and white adipose tissue in development and function, Front. Physiol. 9 (2018).

[10] I. Rune, et al., Long-term Western diet fed apolipoprotein E-deficient rats exhibit only modest early atherosclerotic characteristics, Sci. Rep. 8 (2018).

[11] J.M. Tarkin, F.R. Joshi, J.H.F. Rudd, PET imaging of inflammation in atherosclerosis, Nat. Rev. Cardiol. 11 (2014) 443–457.

[12] D. Rosenbaum, A. Millon, Z.A. Fayad, Molecular imaging in atherosclerosis: FDG PET, Curr. Atheroscler. Rep. 14 (2012) 429–437.

[13] N.R. Evans, J.M. Tarkin, M.M. Chowdhury, E.A. Warburton, J.H.F. Rudd, PET imaging of atherosclerotic disease: advancing plaque assessment from anatomy to pathophysiology, Curr. Atheroscler. Rep. 18 (2016).

[14] M.G. Masteling, et al., High-resolution imaging of human atherosclerotic carotid plaques with micro18F-FDG PET scanning exploring plaque vulnerability, J. Nucl. Cardiol. 18 (2011) 1066–1075.

[15] N. Percie du Sert, et al., The ARRIVE guidelines 2.0: updated guidelines for reporting animal research, PLoS Biol. 18 (2020), e3000410.

[16] S. Berenji Ardestani, V.V. Matchkov, I. Eftedal, M. Pedersen, A single simulated Heliox dive modifies endothelial function in the Vascular Wall of ApoE knockout male rats more than females, Front. Physiol. 10 (2019).

[17] T.D. Nguyen, F.F. Hållenius, X. Lin, M. Nyman, O. Prykhodko, Monobutyrin and Monovalerin affect brain short-chain fatty acid profiles and tight-junction protein expression in ApoE-knockout rats fed high-fat diets, Nutrients 12 (2020) 1202.

[18] R. Golestani, et al., Small-animal SPECT and SPECT/CT: application in cardiovascular research, Eur. J. Nucl. Med. Mol. Imaging 37 (2010) 1766–1777.

[19] K.J. Livak, T.D. Schmittgen, Analysis of relative gene expression data using real-time quantitative PCR and the 2(-Delta Delta C(T)) method, Methods San Diego Calif 25 (2001) 402–408.

[20] H. Buikema, et al., Cardiovascular physiology: the deletion polymorphism of the angiotensin-converting enzyme gene is related to phenotypic differences in human arteries, Eur. Heart J. 17 (1996) 787–794.

[21] J.E. Gilda, A.V. Gomes, Stain-free total protein staining is a superior loading control to β-actin for Western blots, Anal. Biochem. 440 (2013) 186–188.

[22] A.J. Fosang, R.J. Colbran, Transparency is the key to quality, J. Biol. Chem. 290 (2015) 29692–29694.

[23] G.M. Aldridge, D.M. Podrebarac, W.T. Greenough, I.J. Weiler, The use of total protein stains as loading controls: an alternative to high-abundance single-protein controls in semi-quantitative immunoblotting, J. Neurosci. Methods 172 (2008) 250–254.

[24] L. Lorenz, et al., Mechanosensing by β1 integrin induces angiocrine signals for liver growth and survival, Nature 562 (2018) 128–132.

[25] R.C. Orchard, C.B. Wilen, H.W. Virgin, Sphingolipid biosynthesis induces a conformational change in the murine norovirus receptor and facilitates viral infection, Nat. Microbiol. 3 (2018) 1109–1114.

[26] Y. Zhao, et al., Hyperlipidemia induces typical atherosclerosis development in Ldlr and Apoe deficient rats, Atherosclerosis 271 (2018) 26–35.

[27] R. Hachani, et al., Hypercholesterolemic diet induces vascular smooth muscle cell apoptosis in sympathectomized rats via intrinsic pathway, Auton. Neurosci. 183 (2014) 49–57.

[28] S. Sethi, O. Rivera, R. Oliveros, R. Chilton, Aortic stiffness: pathophysiology, clinical implications, and approach to treatment, Integr. Blood Press. Control 29 (2014), https://doi.org/10.2147/IBPC.S59535.

[29] D.S. Farias-Itao, et al., B lymphocytes and macrophages in the perivascular adipose tissue are associated with coronary atherosclerosis: an autopsy study, J. Am. Heart Assoc. 8 (2019).

[30] M. Son, et al., Ecklonia cava extract attenuates endothelial cell dysfunction by modulation of inflammation and Brown adipocyte function in perivascular fat tissue, Nutrients 11 (2019) 2795.

[31] X. Wang, et al., Macrophage inducible nitric oxide synthase circulates inflammation and promotes lung carcinogenesis, Cell Death Discov. 4 (2018).

[32] R. Nosalski, T.J. Guzik, Perivascular adipose tissue inflammation in vascular disease: PVAT inflammation in vascular disease, Br. J. Pharmacol. (2017), https://doi.org/10.1111/bph.13705.

[33] G.S. Getz, C.A. Reardon, ApoE knockout and knockin mice: the history of their contribution to the understanding of atherogenesis, J. Lipid Res. 57 (2016) 758–766.

[34] J. Sijbesma, et al., Characterization of the apolipoprotein E-deficient rat as novel model for atherosclerosis imaging, Eur. J. Nucl. Med. Mol. Imaging 46 (2019) S248–S249.

[35] T.A.M. Almabrouk, et al., High fat diet attenuates the Anticontractile activity of aortic PVAT via a mechanism involving AMPK and reduced adiponectin secretion, Front. Physiol. 9 (2018).

[36] W. Xiong, et al., Brown adipocyte-specific PPARγ (peroxisome proliferator-activated receptor γ) deletion impairs perivascular adipose tissue development and enhances atherosclerosis in mice, Arterioscler. Thromb. Vasc. Biol. 38 (2018) 1738–1747.

[37] S.U. Amano, et al., Local proliferation of macrophages contributes to obesity-associated adipose tissue inflammation, Cell Metab. 19 (2014) 162–171.

[38] K. Tanaka, M. Sata, Roles of perivascular adipose tissue in the pathogenesis of atherosclerosis, Front. Physiol. 9 (2018).

[39] S.N. Saxton, et al., Perivascular adipose tissue contributes to the modulation of vascular tone in vivo, J. Vasc. Res. 56 (2019) 320–332.

[40] Y. Hada, et al., Selective purification and characterization of adiponectin multimer species from human plasma, Biochem. Biophys. Res. Commun. 356 (2007) 487–493.

[41] M. Durik, et al., Nucleotide excision DNA repair is associated with age-related vascular dysfunction, Circulation 126 (2012) 468–478.

[42] V. Tran, et al., The vascular consequences of metabolic syndrome: rodent models, endothelial dysfunction, and current therapies, Front. Pharmacol. 11 (2020) 148.

[43] M. Hohl, et al., Modulation of the sympathetic nervous system by renal denervation prevents reduction of aortic distensibility in atherosclerosis prone ApoE-deficient rats, J. Transl. Med. 14 (2016).

[44] S. Kagota, et al., Perivascular adipose tissue-enhanced vasodilation in metabolic syndrome rats by Apelin and N-acetyl–l-cysteine-sensitive factor(s), Int. J. Mol. Sci. 20 (2018) 106.

[45] N. Xia, et al., Uncoupling of endothelial nitric oxide synthase in perivascular adipose tissue of diet-induced obese mice, Arterioscler. Thromb. Vasc. Biol. 36 (2016) 78–85.

[46] N. Xia, et al., Restoration of perivascular adipose tissue function in diet-induced obese mice without changing bodyweight: uncoupling of obesity from vascular dysfunction, Br. J. Pharmacol. 174 (2017) 3443–3453.

[47] R.G. Knowles, S. Moncada, Nitric oxide synthases in mammals, Biochem. J. 298 (1994) 249–258.

[48] C.A. Taylor, T.J.R. Hughes, C.K. Zarins, Finite element modeling of three-dimensional pulsatile flow in the abdominal aorta: relevance to atherosclerosis, Ann. Biomed. Eng. 26 (1998) 975–987.

[49] Z.A. Fayad, et al., In vivo magnetic resonance evaluation of atherosclerotic plaques in the human thoracic aorta: A comparison with transesophageal echocardiography, Circulation 101 (2000) 2503–2509.

[50] J. Padilla, N.T. Jenkins, V.J. Vieira-Potter, M.H. Laughlin, Divergent phenotype of rat thoracic and abdominal perivascular adipose tissues, Am. J. Physiol. Regul. Integr. Comp. Physiol. 304 (2013) R543–R552.

[51] M. Barton, et al., Endothelin ETA receptor blockade restores NO-mediated endothelial function and inhibits atherosclerosis in apolipoprotein E-deficient mice, Proc. Natl. Acad. Sci. 95 (1998) 14367–14372.

[52] W.N. Nowak, J. Deng, X.Z. Ruan, Q. Xu, Reactive oxygen species generation and atherosclerosis, Arterioscler. Thromb. Vasc. Biol. 37 (2017).

[53] M. Friederich-Persson, A. Nguyen Dinh Cat, P. Persson, A.C. Montezano, R. M. Touyz, Brown adipose tissue regulates small artery function through NADPH oxidase 4–derived hydrogen peroxide and redox-sensitive protein kinase G-1α, Arterioscler. Thromb. Vasc. Biol. 37 (2017) 455–465.